Generating non-Rayleigh speckles with tailored intensity statistics

Yaron Bromberg* and Hui Cao†
Department of Applied Physics, Yale University, New Haven, Connecticut 06520 USA

We experimentally generate speckle patterns with non-Rayleigh intensity statistics using a phase-only spatial light modulator. By introducing high order correlations to the input light fields we redistribute the intensity among the speckle grains, while preserving the granular structure of the pattern. Our method is versatile and allows for generating speckle patterns with enhanced or diminished contrast in a controlled manner.

arXiv:1401.7662v2 [physics.optics] 20 Mar 2014

Speckle patterns appear whenever a coherent wave impinges upon a scattering sample. The granular structure of speckles results from the sensitivity of the interference pattern to the relative phases of the scattered partial waves. As speckle formation is essentially a wave phenomena, it has been observed for a wide range of waves of different nature, including ultrasonic waves [1], microwaves [2, 3], optical waves [4], X-rays [5], and matter waves [6]. In spite of the diverse settings in which speckles appear, they usually show universal statistical properties. The apparent random distribution of the intensity mostly follows Rayleigh statistics, i.e. the probability density function of the intensity is a negative exponential [4]. An interesting question is whether the spatial structure of speckle patterns necessarily dictates Rayleigh statistics, or perhaps it is possible to tailor the distribution of the intensities among the speckle grains while maintaining the random granular pattern?

The reason that speckle patterns typically exhibit Rayleigh statistics is that Rayleigh statistics emerge under rather general conditions: the field is a sum of a large number of partial waves with independently varying amplitudes and phases, and the phases are uniformly distributed over a range of 2π. In the weak scattering regime the latter condition is not satisfied, hence non-Rayleigh speckles with a low contrast and a strong DC background are formed [7]. Similarly, in the near-field zone of a scattering media where just a small number of scattered partial waves is detected and the relative phase of these waves does not cover the full 2π range, low contrast speckles with nonuniversal statistics are observed [8–10]. In the strong scattering regime where the phases are uniformly distributed, deviations from Rayleigh statistics can be observed for a small number of partial waves, but the statistics approaches Rayleigh statistics as the number of partial waves is increased [11]. For generating speckles with robust non-Rayleigh statistics that result from redistribution of the intensity among the speckle grains, we need to consider the interference of a large number of partial waves whose phases are uniformly distributed over a range of 2π. In this case the only way to observe non-Rayleigh speckles is to make the complex amplitudes of the partial waves statistically dependent. Multiple scattering can introduce mesoscopic correlations that modify Rayleigh statistics due to strong fluctuations in the total power that is transmitted through the sample [12]. However, the intensity distribution for a single random configuration, i.e. the distribution of the intensities between the speckle grains, still follows Rayleigh statistics [13, 14]. Similarly, non-Rayleigh statistics are observed when the total power that is incident on a scattering sample fluctuates [4] or when two identical speckle patterns with a fluctuating relative phase are interfered [15], yet per speckle realization the intensity is Rayleigh distributed. We on the other hand are seeking to redistribute the intensities among the speckle grains, so that each individual pattern will show non-Rayleigh statistics and not just the ensemble average.

In this Letter we show how to tailor the speckle statistics using a phase-only spatial light modulator (SLM) that is illuminated by a laser beam. The SLM pixels mimic scattering from a rough surface, and the diffraction from each pixel corresponds to a partial wave that is scattered from the SLM plane. We record the speckle patterns at the Fourier plane of the SLM, where the intensity statistics are determined by the statistical properties of the phase matrices that are applied to the SLM. We developed a simple method for finding the phase matrices that yield non-Rayleigh speckles, which we use for tailoring the intensity distribution between the speckle grains. Since speckle patterns are a valuable resource for both fundamental research [2, 13, 14, 16–20] and numerous applications [21–29], a control of the intensity statistics can have a dramatic impact on the way we use and analyze speckles. For example one can utilize tailored speckles to synthesize the statistics of disordered optical potentials for cold atoms and colloidal particles [30–32], or optimize the intensity statistics per application in speckle illumination imaging [26–29]. As speckle patterns are intimately related to the statistical properties of thermal light sources, temporally fluctuating non-Rayleigh speckles may also be regarded as a pseudothermal light source. Such a source violates the Siegert relation and exhibits a bunching factor $g^{(2)}(0) \neq 2$, which enables exploring classical models of extra-bunching [33, 34] and high-order ghost imaging [35].

To experimentally demonstrate our method for generating non-Rayleigh speckles, we start with an example for enhancing the contrast of a speckle pattern. We use a phase-only reflective SLM, which is illuminated by a lin-

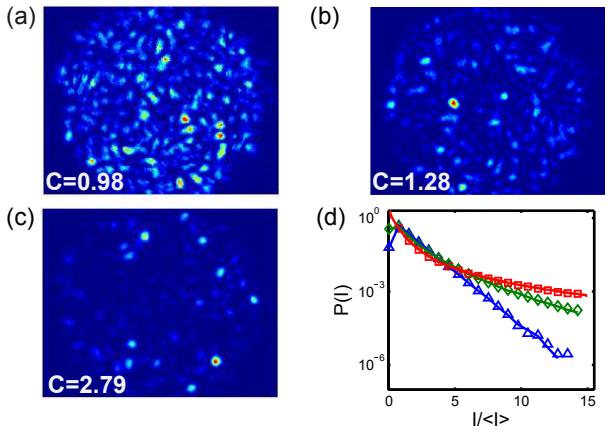

Figure 1. Experimental generation of super-Rayleigh speckles. (a) - (c) Images of the speckle patterns at the Fourier plane of the SLM, and (d) the corresponding intensity distribution function. (a) Standard Rayleigh speckles with a contrast of C=0.98 and a negative exponential intensity distribution ((d), blue triangles). (b) Super-Rayleigh speckles with a contrast of C=1.28, and an intensity distribution that decays slower than the negative exponential ((d), green diamonds). The light is concentrated at a fewer speckles grains compared to (a), yielding non-Rayleigh statistics. (c) Higher contrast super-Rayleigh speckles with C=2.79 and a long tailed intensity histogram ((d), red squares). Solid lines are histograms obtained for the normalized speckle patterns (see text).

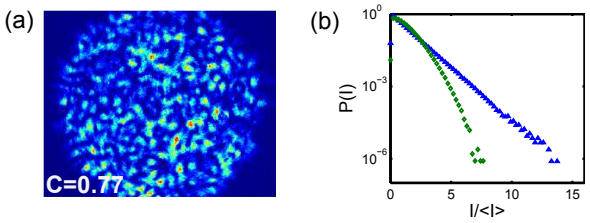

Figure 2. (a) A speckle pattern measured at the Fourier plane of the SLM, using a phase matrix that was designed to generate sub-Rayleigh speckles. The low contrast of the pattern results from a more homogenous distribution of the intensity among the speckle grains compared to Rayleigh speckles. (b) Measured intensity distribution function of the sub-Rayleigh speckles (green diamonds), which decays much faster than the negative exponential observed for Rayleigh speckles (blue triangles).

early polarized laser beam with diameter D=5mm. The SLM pixels are grouped to macro pixels providing a control over 3000 independent phase elements. We place the SLM at the front focal plane of a lens and record the intensity pattern at the Fourier plane of the SLM by imaging the back focal plane of the lens (see [36] for additional details). When we apply to the SLM a random uncorrelated phase matrix a Rayleigh speckle pattern is observed at the Fourier plane (figure 1a). To generate a speckle pattern with an enhanced contrast, we must send to the SLM a phase matrix with correlated pixels. To find such a matrix, we first numerically generate a high contrast speckle, for example by squaring the field of a standard Rayleigh speckle, $E^2_{Ray}(x,y)$. Next, we compute the inverse Fourier transform, and apply the phase of the inverse Fourier transform to the SLM. Figure 1b shows the resulting speckle pattern of a phase matrix computed in this way. It is clearly seen that the distribution of the intensities among the speckle grains is different than for Rayleigh speckles (figure 1a), a few grains are much brighter than the rest. Indeed the intensity histogram collected from a 1000 speckle realizations decays slower than a negative exponential, featuring the high probability to obtain bright speckle grains (figure 1d, green diamonds). The contrast of the patterns, defined as $C = \sqrt{\langle I^2 \rangle / \langle I \rangle^2 - 1}$ where $\langle \cdots \rangle$ denotes spatial and ensemble averaging, is C=1.28, significantly higher than the contrast measured for the Rayleigh speckles C=0.98. We coin this kind of high contrast patterns *super-Rayleigh* speckles.

Instead of squaring the Rayleigh speckle field E_{Ray} as in the example above, in principle we can use any nonlinear transformation $h(E_{Ray})$ to obtain non-Rayleigh speckle. Thus we can generate super-Rayleigh speckles with a higher contrast by using, for example, the fourth power of the speckle field $h(E_{Ray}) = E^4_{Ray}$. We send to the SLM the phase of the inverse Fourier transform of E^4_{Ray}, and observe patterns with C=2.79 (figure 1c) and a long tailed intensity histogram (figure 1d, red squares). We note that the long tailed intensity histograms of super-Rayleigh speckles result from redistribution of the intensity among the speckle grains and not because of fluctuations in the total intensity of different speckle realizations. To verify this, we normalize all the speckle patterns to have the same total intensity, and show that the intensity histograms of the normalized and non-normalized patterns are identical (figure 1d, solid lines).

The super-Rayleigh speckle statistics arises from concentrating the light to a fewer bright grains compared to Rayleigh speckles. It is interesting to explore the opposite regime which we coin *sub-Rayleigh* speckles, where the light is distributed in a more homogenous manner among the grains. Intuitively, saturation of the intensity can reduce the intensity fluctuations and the speckle contrast, while preserving the granular structure of the speckles. Thus we use a nonlinear transformation that saturates the amplitude of a Rayleigh speckle, but keeps its phase untouched, $h(E_{Ray}) = \sqrt{1-e^{-|E_{Ray}|^2}}e^{i\theta_{Ray}}$ where $\theta_{Ray} = arg(E_{Ray})$ is the phase of the Rayleigh speckle field. Unlike super-Rayleigh speckles, where we applied to the SLM the phase of the inverse Fourier transform of $h(E_{Ray})$ and observed a pattern that to a good approximation matched $h(E_{Ray})$, for sub-Rayleigh speckles when we keep only the phase of the inverse Fourier transform of $h(E_{Ray})$ and disregard the amplitude varia-

tion, we observe nearly standard Rayleigh speckles. This is because the amplitude modulation encodes much information of the transformed speckle. To transfer this information to phase modulation, we apply an iterative procedure based on the Gershberg-Saxton algorithm [37], where using Fourier transforms we numerically propagate the field back and forth between the SLM plane and the Fourier plane. At each iteration step we fix the amplitude at the Fourier plane to be $\sqrt{1-e^{-|E_{Ray}|^2}}$, and we set the amplitude at the SLM plane to match the amplitude of the beam profile that impinges on the SLM. After 50 iterations the algorithm converges to a speckle pattern at the Fourier plane with an intensity pattern that is proportional to $1-e^{-|E_{Ray}|^2}$ and a corresponding phase matrix at the SLM plane. We repeat the algorithm with different initial Rayleigh speckles E_{Ray} to generate a set of a phase matrices, which we then send to the SLM. The recorded patterns indeed show a low contrast (C=0.77), and the intensity histogram decays faster than a negative exponential (figure 2). By comparing figure 2a to figure 1a, it can be seen that intensity distribution among the speckle grains of the sub-Rayleigh speckles is more homogenous, which is the origin of the lower contrast.

One interesting feature of the non-Rayleigh speckles is that the speckle statistics changes as the beam propagates. All the results presented so far were measured at the Fourier plane of the SLM, however, when we scan the image plane away from the Fourier plane, the speckles gradually return to Rayleigh statistics [36]. Figure 3 shows the contrast of the recorded speckle patterns as a function of the distance between the Fourier plane and the plane that is imaged by the camera, showing that the contrast of the super-Rayleigh and sub-Rayleigh speckles is axially dependent, whereas the contrast of the Rayleigh speckle remains constant. The range over which the non-Rayleigh statistics are observed corresponds to the longitudinal length of a single speckle. This longitudinal length is equal to the Rayleigh range of an input Gaussian beam that is focused to a spot of the size of a single speckle [38]. It is therefore determined by the envelope of the beam that illuminates the SLM, and it is not modified by phase-only modulation.

Observing non-Rayleigh statistics necessarily implies that the fields at the SLM plane break at least one of the two conditions for observing Rayleigh speckles: either the phases are not uniformly distributed over 2π, or the fields at different pixels are correlated. Figure 4a shows the histograms of the phases that were used to generate Rayleigh speckles (blue triangles), super-Rayleigh speckles (green diamonds) and sub-Rayleigh speckles (red squares). All three histograms are constant over $[0,2\pi]$, which means that the non-Rayleigh statistics must originate from correlations between the SLM pixels. We therefore look at the correlation of the field at the SLM plane $G^{(1)}_{SLM}(\Delta_x,\Delta_y) = \langle E_{SLM}(x,y)E^*_{SLM}(x+\Delta_x,y+\Delta_y)\rangle$. We obtain $G^{(1)}_{SLM}$ using the Wiener-Khinchin theorem [39], by computing the Fourier transform of the averaged intensity pattern at the Fourier plane of the SLM. The $G^{(1)}_{SLM}$ curves for super- and sub-Rayleigh speckles are presented in figure 4b, showing that fields at different macropixels are uncorrelated. The question is then how can uncorrelated fields with phases that are uniformly distributed over 2π yield non-Rayleigh statistics? The answer is that $G^{(1)}_{SLM}(\Delta)=0$ indicates that fields separated by a distance Δ are uncorrelated, but it does not necessarily mean that the fields are statistically independent. For non-Gaussian random fields, higher order correlations can exist even if the first order correlation vanishes [39].

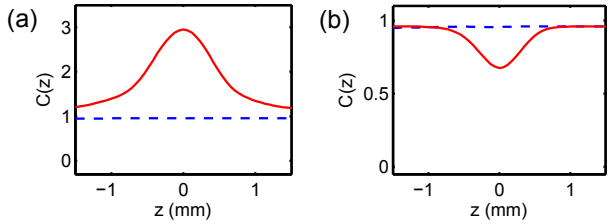

Figure 3. Axially dependent speckle contrast. (a) The measured contrast of the speckle patterns versus the distance from the Fourier plane, for Rayleigh (blue dashed line), and super-Rayleigh (red line) speckles. (b) Same as (a) for sub-Rayleigh speckles. The width of the contrast peak or dip corresponds to the longitudinal length of a single speckle.

To investigate the role of higher order correlations in the formation of non-Rayleigh speckles, we study numerically the contribution of the second-order field correlations to the contrast of the speckle patterns. Since the laser beam is linearly polarized and the scattering angles from the SLM are too small to introduce radial polarization, we consider scalar fields. A partial wave that diffracts from an SLM pixel at position $\mathbf{r}$ to position $\boldsymbol{\rho}$ in the Fourier plane is proportional to $e^{i(\psi_{\mathbf{r}}-2\pi\boldsymbol{\rho}\mathbf{r}/\lambda f)}$, where $\psi_{\mathbf{r}}$ represents the SLM phase at $\mathbf{r}$. The square of the contrast of the speckle pattern at the Fourier plane is therefore:

$$C^2 \equiv \langle I^2\rangle - \langle I\rangle^2 = \left\langle \int d^2\boldsymbol{\rho}|E(\boldsymbol{\rho})|^4 \right\rangle_e - 1 \qquad (1)$$
$$= \frac{1}{N^2}\sum_{\mathbf{r_1},\mathbf{r_2},\mathbf{r_3}\mathbf{r_4}} \left\langle \mathbf{e}^{\mathbf{i}(\psi_{\mathbf{r1}}+\psi_{\mathbf{r2}}-\psi_{\mathbf{r3}}-\psi_{\mathbf{r4}})}\right\rangle_{\mathbf{e}} \delta_{\mathbf{r_1}+\mathbf{r_2}-\mathbf{r_3},\mathbf{r_4}} - 1$$

where N is the number of SLM pixels, $\langle\cdots\rangle_e$ denotes ensemble averaging, and $\langle I\rangle$ is normalized to 1. The sum on the right hand side is in fact a sum over the second order correlation between the fields at all the SLM pixels: $\sum G^{(2)}_{SLM}(\mathbf{r_1},\mathbf{r_2},\mathbf{r_3},\mathbf{r_1}+\mathbf{r_2}-\mathbf{r_3})$. We can decompose this sum into 4 terms, $C^2=\Gamma^{(2)}_1+\Gamma^{(2)}_2+\Gamma^{(2)}_3+\Gamma^{(2)}_4-1$, where $\Gamma^{(2)}_p$ is the second order correlation between fields at p *different* pixels, e.g. $\Gamma^{(2)}_4 = \sum_{\mathbf{r_1}\neq\mathbf{r_2}\neq\mathbf{r_3}\neq\mathbf{r_4}} G^{(2)}_{SLM}(\mathbf{r_1},\mathbf{r_2},\mathbf{r_3},\mathbf{r_4}=\mathbf{r_1}+\mathbf{r_2}-\mathbf{r_3})$. For

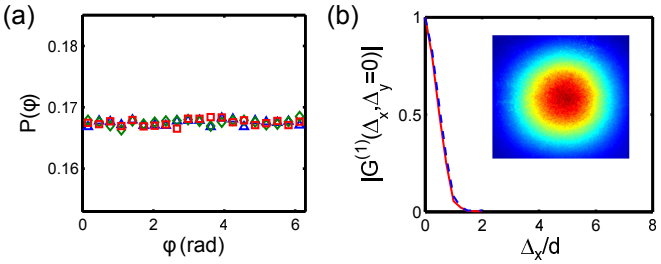

Figure 4. (a) Histograms of the phases used to generate Rayleigh (blue triangles), super-Rayleigh (green diamonds) and sub-Rayleigh (red squares) speckles. All three histograms are constant over 2π. (b) The field correlation at the SLM plane $G^{(1)}_{SLM}$ for super-Rayleigh speckle (blue dashed line) and sub-Rayleigh speckle (red solid line). $d = 80\mu m$ is the size of one macro pixel. Fields separated by more than one macropixel are uncorrelated, indicating that the source of the non-Rayleigh statistics is in higher order correlations. The inset shows the average intensity for the sub-Rayleigh speckles, from which $G^{(1)}_{SLM}$ was computed.

Rayleigh speckles that are formed by statistically independent pixels, only correlations of fields at the same pixel contribute to the sum, hence $\Gamma^{(2)}_1 = 1/N$, $\Gamma^{(2)}_2 = 2 - 2/N$ and $\Gamma^{(2)}_3 = \Gamma^{(2)}_4 = 0$. For non-Rayleigh speckles, we evaluate $\Gamma^{(2)}_p$ numerically by calculating the second order correlations $G^{(2)}_{SLM}(\mathbf{r_1}, \mathbf{r_2}, \mathbf{r_3}, \mathbf{r_4} = \mathbf{r_1} + \mathbf{r_2} - \mathbf{r_3})$ for all the combinations of the indices $\{\mathbf{r_1}, \mathbf{r_2}, \mathbf{r_3}, \mathbf{r_4}\}$, and decomposing the results into the four terms $\Gamma^{(2)}_p$ according to the number of different indices that appear in each combination. The numerical results for 5000 phase patterns with 100 pixels are summarized in Table 1. It is seen that the source of the non-Rayleigh statistics is $\Gamma^{(2)}_4$, i.e. the cross-correlation between four *different* pixels.

In Eq. (1) the high order correlations of the field at the SLM plane are linked to the intensity statistics at the Fourier plane. However, for points that are not in the Fourier plane an additional quadratic phase factor $e^{i\pi z(\mathbf{r_1^2}+\mathbf{r_2^2}-\mathbf{r_3^2}-\mathbf{r_4^2})/\lambda f^2}$ multiplies each term in the right hand side of Eq. (1), where z is axial the distance from the Fourier plane. Due to this quadratic phase the high order correlations do not add in phase and their contribution to the intensity statistics vanishes. This is the reason why we observe non-Rayleigh statistics only at the Fourier plane of the SLM. We note that by adding a quadratic phase to the SLM it is possible to shift the axial position of the Fourier plane where the speckle statistics is non-Rayleigh.

In conclusion, we developed a method to generate speckle patterns with controlled intensity statistics. In contrast to previous works which used an SLM to control the spatial coherence of light fields by shaping the spatial frequency distribution [40–42] or synthesizing the coherent mode decomposition of the field [43], we use the SLM to redistribute the intensity among the speckle grains. We link the observed non-Rayleigh statistics to higher order correlations of the scattered partial waves, paving the way towards a better understanding of the information carried by speckles that are scattered from disordered samples with structural correlations. Non-Rayleigh speckles also offer new opportunities for speckle illumination applications. On one hand, the axially varying contrast of super-Rayleigh speckles can be utilized for achieving better optical sectioning in speckle illumination microscopy. On the other hand, the homogenous distribution of sub-Rayleigh speckles are attractive for imaging modalities that utilize speckle illumination, as it can reduce the number of projections required for averaging the speckles to observe a smooth image and enhance the image acquisition rate. Therefore, tailored speckles allows optimizing the intensity statistics for target applications.

	$\Gamma^{(2)}_1$	$\Gamma^{(2)}_2$	$\Gamma^{(2)}_3$	$\Gamma^{(2)}_4$
Rayleigh	0.0	2.0	0.0	**0.0**
Super-Rayleigh$h(E) = E^2$	0.0	2.0	0.0	**0.7**
Super-Rayleigh$h(E) = E^4$	0.0	2.0	0.0	**5.6**
Sub-Rayleigh	0.0	2.0	0.0	**-0.4**

Table I. Numerical evaluation of $\Gamma^{(2)}_p$, the second order correlation between fields at p different pixels, for speckles of different statistics. The cross-correlation between fields at four different pixels $\Gamma^{(2)}_4$ is the source of the non-Rayleigh statistics.

We thank Eric Dufresne, Brandon Redding, Sebastien Popoff and Arthur Goetschy for fruitful discussions. This work is supported partially by NSF under the Grant Nos. ECCS1128542 and DMR1205307.

* yaron.bromberg@yale.edu
† hui.cao@yale.edu

[1] R. Wagner, S. Smith, J. Sandrik, H. Lopez; IEEE Trans Sonics Ultrasonics. 30, 156-163 (1983).
[2] J. Wang and A. Z. Genack, Nature 471, 345–348 (2011).
[3] J. S. Lee, . Computer Graphics and Image Processing, 17, 24-32 (1981).
[4] J. W. Goodman, Speckle Phenomena in Optics: Theory and Applications (Roberts and Co., Englewood, 2007).
[5] M. Sutton, S. G. J. Mochrie, T. Greytak, S. E. Nagler, and L. E. Berman, Nature 253, 618-610 (1991).
[6] R.G. Dall, S.S. Hodgman, A.G. Manning, M.T. Johnsson, K.G.H. Baldwin A.G. Truscott, Nat. Commun. 2, 291 (2011).
[7] W. T. Welford, Contemp. Physics. 21, 401-412 (1980).
[8] J.-J. Greffet and R. Carminati, Ultramicroscopy 61, 43 (1995).
[9] A. Apostol and A. Dogariu, Phys. Rev. Lett., 91 093901 (2003).
[10] A. Apostol and A. Dogariu, Pheys Rev. E 72, 05602(R) (2005).

[11] J. W. Goodman, Appl. Opt. 47, A111 (2008).
[12] T. M. Nieuwenhuizen and M. C. W. van Rossum, Phys. Rev. Lett. 74, 2674 (1995).
[13] A. Z. Genack and A. A. Chabanov, J. Phys. A, 38, 10465-10488 (2005).
[14] T. Strudley, T. Zehender, C. Blejean, E. P. A. M. Bakkers and O. L. Muskens, Nature Phot. 7, 413 (2013).
[15] P. Hong, J. Liu, and G. Zhang, Phys. Rev. A 86, 013807 (2012).
[16] F. Scheffold and G. Maret, Phys. Rev. Lett., 81, 5800 (1998).
[17] F. Ferri, D. Magatti, A. Gatti, M. Bache, E. Brambilla, and L. A. Lugiato, Phys. Rev. Lett. 94, 183602 (2005).
[18] D. J. Pine, D. A. Weitz, P. M. Chaikin and E. Herbolzheimer, Phys. Rev. Lett. 60, 1134 (1988).
[19] W. Langbein, J. M. Hvam, and R. Zimmermann, Phys. Rev. Lett. 82, 1040 (1999).
[20] T. Schwartz, G. Bartal, S. Fishman, and M. Segev, Nature (London) 446, 52 (2007).
[21] D. A. Boas and A. K. Dunn, J. Biomed. OSLMpt. 15 011109 (2010).
[22] A.C. Völker, P. Zakharov, B. Weber, F. Buck and F. Scheffold, Opt. Exp. 13, 9782 (2005).
[23] F. Scheffold and I. D. Block, Optics Express, 20, 192 (2011).
[24] N. Curry, P. Bondareff, M. Leclercq, N. F. van Hulst, R. Sapienza, S. Gigan and S. Grésillon, Opt. Lett. 36, 3332 (2013).
[25] B. Redding, S. F. Liew, R. Sarma, and H. Cao, Nat. Photonics 7, 746 (2013).
[26] M.C. Pitter C. W. See, and M. G. Somekh, Opt. Lett. 29, 1200 (2004).
[27] E. Mudry, K. Belkebir, J. Girard, J. Savatier, E. Le Moal, C. Nicoletti, M. Allain, and A. Sentenac, Nat. Photonics 6, 312 (2012).
[28] D. Lim, K. K. Chu, and J. Mertz, Opt. Lett. 33, 1819-1821 (2008) .
[29] J. Gateau, T. Chaigne., O. Katz, S. Gigan and E. Bossy, Opt Lett. 38, 5188-5191 (2013).
[30] J. Billy, V. Josse, Z. Zuo, A. Bernard, B. Hambrecht, P. Lugan, D. Clément, L. Sanchez-Palencia, P. Bouyer, and A. Aspect, Nature 453, 891 (2008).
[31] K. M. Douglass, S. Sukhov, and A. Dogariu, Nat. Photonics 6, 834 (2012).
[32] G. Volpe, G. Volpe and S. Gigan, Sci. Rep. 4, 3936 (2014).
[33] F. Boitier, A. Godard, N. Dubreuil, P. Delaye, C. Fabre, and E. Rosencher, Nat. Commun. 2, 425 (2011).
[34] T. S. Iskhakov, A. Perez, K. Y. Spasibko, M. V. Chekhova, and G. Leuchs, Opt. Lett. 37, 1919 (2012).
[35] K. W. C. Chan, M. N. O'Sullivan, and R. W. Boyd, Opt. Express 18, 5562 (2010).
[36] Supplemental Material
[37] R. W. Gerchberg and W. O. Saxton, Optik 35, 237 (1972).
[38] A. Gatti, D. Magatti, and F. Ferri, Phys. Rev. 78, 063806 (2008).
[39] L. Mandel and E. Wolf, Optical Coherence and Quantum Optics (Cambridge, United Kingdom, 1995).
[40] H. Funamizu and J. Uozumi, Opt. Express 15, 7415 (2007).
[41] L. Waller, B. Situ and J. W. Fleischer, Nature Photonics 6, 474-479 (2012).
[42] C. Sun, L. Waller, D. V. Dylov, and J. W. Fleischer, Phys. Rev. Lett., 108, 263902 (2012).
[43] B. Rodenburg, M. Mirhosseini, O. S. Magaña-Loaiza, R. W. Boyd, arXiv:1312.6878 (2013).

arXiv:1401.7662v2 [physics.optics] 20 Mar 2014

Supplementary Material: Generating non-Rayleigh speckles with tailored intensity statistics

Yaron Bromberg* and Hui Cao†
Department of Applied Physics, Yale University, New Haven, Connecticut 06520 USA

EXPERIMENTAL SETUP

A phase-only reflective SLM (Hamamatsu, LCOS-SLM) is illuminated by a collimated linearly polarized laser beam (Coherent OBIS, λ=640nm), which is expanded and clipped by an iris to uniformly cover a circular area on the SLM with diameter D=5mm. As shown schematically in figure S1, the SLM pixels are grouped to macropixels with a pitch of $80\mu m$, providing a control over 3000 independent phase elements. The SLM is placed at the front focal plane of a lens L_1 (f_1=50cm), and the back focal plane of the lens is re-imaged onto a 12bit CCD camera (Manta, Allied Vision) using 2 lenses, L_2 and L_3, in a 4f configuration (f_2=10cm, f_3=15cm). Axial scans of the image plane was performed by adding to the beam path two identical microscope objectives (x10, NA=0.25) and scanning the position of one of the objectives using a motorized stage.

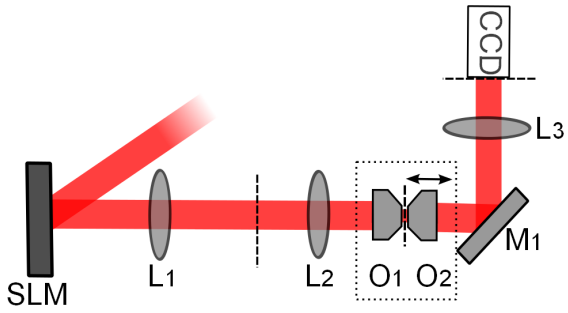

Figure S 1. Schematic of the experimental setup. A phase-only SLM is placed at the front focal plane of a lens (L_1). The Fourier transform of the SLM plane is formed at the back focal plane of L_1, and is reimaged onto a CCD camera using a pair of lens (L_2,L_3) in a 4f configuration. The axial variation of the speckle pattern was recorded by inserting a pair of identical microscope objectives (O_1,O_2) after lens L_2, and scanning the axial position of O_2 using a motorized stage. The dashed lines mark the Fourier plane and its two conjugated planes.

THREE DIMENSIONAL PATTERN OF NON-RAYLEIGH SPECKLES

The non-Rayleigh speckles have a non-homogenous three-dimensional structure, the deviation from Rayleigh statistics is observed only in the vicinity of the Fourier plane of the SLM. Images of the patterns measured at the Fourier plane, and 3mm away from the Fourier plane are presented in Figure S2. While the patterns of the super-Rayleigh and sub-Rayleigh speckles clearly exhibit non-Rayleigh statistics at the Fourier plane, away from the Fourier plane they resemble standard speckle patterns with Rayleigh statistics. Movies showing the the transition from the non-Rayleigh to the Rayleigh statistics as the speckle propagates are recorded by scanning the axial position of the plane that is imaged onto the camera, and attached [1].

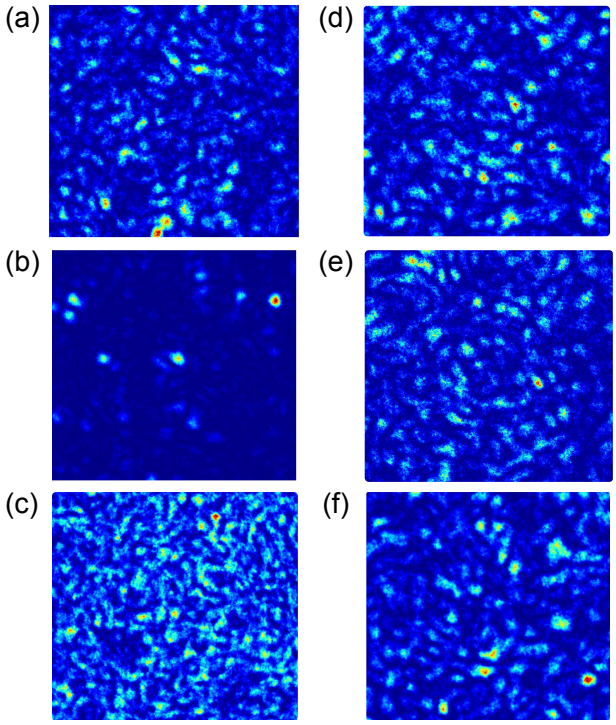

Figure S 2. Images recorded at the Fourier plane (left column), and 3mm away from the Fourier plane (right column), for Rayleigh and non-Rayleigh speckles. Rayleigh speckles (a,b) show the same statistics in both planes, where as super-Rayleigh (c,d) and sub-Rayleigh (e,f) speckles transform into Rayleigh speckles outside of the Fourier plane.

DEVIATIONS FROM RAYLEIGH STATISTICS OF THE LOCAL CONTRAST

In this section we study whether the non-Rayleigh speckle statistics that we measure are in fact locally Rayleigh statistics, but with a spatially dependent average intensity. We have already shown in the main text that the ensemble averaged intensity of the non-Rayleigh

speckles is spatially homogenous, resulting in a delta like field-field correlations for the field at the SLM plain (figure 4b). This however does not rule out the possibility that the statistics are locally Rayleigh statistics, and that the local averaged intensity changes for different realizations. In order to to check whether this is the case, we perform the following analysis of the experimental data. For each speckle realization, we choose a region of interest (ROI) that is centered around the brightest speckle in the frame. We calculate the local contrast inside the ROI by computing $C_r = \sqrt{\langle I^2 \rangle_s / \langle I \rangle_s^2 - 1}$, where $\langle \cdots \rangle_s$ denotes spatial averaging over the ROI area. Next we compute the ensemble average of C_r over all the speckle realizations $C = \langle C_r \rangle_e$. If the non-Rayleigh statistics originated from local Rayleigh statistics, the local contrast should have been equal to C=1 for some range of sizes of the ROI. In order to find the minimal size of the ROI which covers a sufficient number of speckle grains so that the measure of the local contrast would be statistically meaningful, we compute the local contrast also for the Rayleigh speckles (figure S3, blue dotted line). We find that when the ROI covers more than 40 speckle grains the contrast of the Rayleigh speckle converges to C=1. For this size of the ROI it is clearly seen that the contrast of the super-Rayleigh (green dashed line) and sub-Rayleigh (red solid line) speckles are significantly different than C=1, i.e. even the local contrast shows non-Rayleigh statistics.

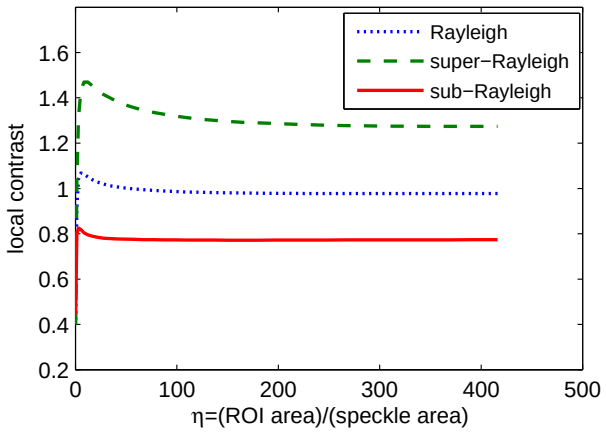

Figure S 3. The local contrast as a function of number of speckle grains in the ROI (defined by the ratio of the ROI area and the speckle grain area). When the area of the ROI contains more than 40 speckle grains ($\eta > 40$), the contrast for Rayleigh speckles converges to 1, indicating that for $\eta > 40$ the definition of the local contrast is statistically meaningful (blue dotted line). In this regime the local contrast of the super-Rayleigh (dashed green line) and sub-Rayleigh (solid red line) speckles exhibits non-Rayleigh statistics, proving that the non-Rayleigh statistics does not result from Rayleigh speckles with a local varying average intensity.

* yaron.bromberg@yale.edu
† hui.cao@yale.edu

[1] See Supplemental Material at [URL will be inserted by publisher] for movies of the three dimensional speckle patterns.